ELSEVIER

Limits on the TeV flux of diffuse gamma rays as measured with the HEGRA air shower array

HEGRA Collaboration

F.A. Aharonian [a], A.G. Akhperjanian [b], J.A. Barrio [c], K. Bernlöhr [a],
H. Bojahr [d], O. Bolz [a], H. Börst [e], J.L. Contreras [c], J. Cortina [f],
S. Denninghoff [f], V. Fonseca [c], H.J. Gebauer [f], J.C. Gonzalez [c],
N. Götting [g], G. Heinzelmann [g], G. Hermann [a], A. Heusler [a],
W. Hofmann [a], D. Horns [g,1], A. Ibarra [c], C. Iserlohe [d], I. Jung [a],
R. Kankanyan [a], M. Kestel [f], J. Kettler [a], A. Kohnle [a],
A. Konopelko [a], H. Kornmayer [f], D. Kranich [f], H. Krawczynski [a],
H. Lampeitl [a], M. Lopez [c], E. Lorenz [f], F. Lucarelli [c], N. Magnussen [d],
O. Mang [e], H. Meyer [d], R. Mirzoyan [f], A. Moralejo [c], E. Oña [c], L. Padilla [c],
M. Panter [a], R. Plaga [f], A. Plyasheshnikov [a,2], J. Prahl [g],
G. Pühlhofer [a], G. Rauterberg [e], W. Rhode [d], A. Röhring [g], G.P. Rowell [a],
V. Sahakian [b], M. Samorski [e], M. Schilling [e], F. Schröder [d], M. Siems [e],
W. Stamm [e], M. Tluczykont [g], H.J. Völk [a], C. Wiedner [a], W. Wittek [f,*]

[a] *Max-Planck-Institut für Kernphysik, Postfach 103980, D-69029 Heidelberg, Germany*
[b] *Yerevan Physics Institute, Alikhanian Br. 2, 375036 Yerevan, Armenia*
[c] *Facultad de Ciencias Físicas, Universidad Complutense, Ciudad Universitaria, E-28040 Madrid, Spain*
[d] *Fachbereich Physik, Universität Wuppertal, Gaußstrasse 20, D-42097 Wuppertal, Germany*
[e] *Institut für Experimentelle und Angewandte Physik, Universität Kiel, Leibnizstraße 15-19, D-24118 Kiel, Germany*
[f] *Max-Planck-Institut für Physik, Föhringer Ring 6, D-80805 München, Germany*
[g] *II. Institut für Experimentalphysik, Universität Hamburg, Luruper Chaussee 149, D-22761 Hamburg, Germany*

* Corresponding author.
E-mail address: wittek@mppmu.mpg.de (W. Wittek).
[1] Present address: Now at Max-Planck-Institut für Kernphysik, Postfach 103980, D-69029 Heidelberg, Germany.
[2] On leave from Altai State University, Dimitrov Street 66, 656099 Barnaul, Russia.

Abstract

Using data from the HEGRA air shower array, taken in the period from April 1998 to March 2000, upper limits on the ratio I_γ/I_{CR} of the diffuse photon flux I_γ to the hadronic cosmic ray flux I_{CR} are determined for the energy region 20–100 TeV. The analysis uses a gamma–hadron discrimination which is based on differences in the development of photon- and hadron-induced air showers after the shower maximum. A method which is sensitive only to the non-isotropic component of the diffuse photon flux yields an upper limit of I_γ/I_{CR} (at 54 TeV) $< 2.0 \times 10^{-3}$ (at the 90% confidence level) for a sky region near the inner galaxy (20° < galactic longitude < 60° and |galactic latitude | < 5°). A method which is sensitive to both the isotropic and the non-isotropic component yields global upper limits of I_γ/I_{CR} (at 31 TeV) $< 1.2 \times 10^{-2}$ and I_γ/I_{CR} (at 53 TeV) $< 1.4 \times 10^{-2}$ (at the 90% confidence level). © 2002 Elsevier Science B.V. All rights reserved.

Keywords: Cosmic rays; Diffuse gamma-ray galactic emission; Gamma rays: observations

1. Introduction

The flux of the diffuse photon background radiation, its spectrum and its evolution with time are very interesting topics of astrophysics. In nearly all energy regions both an extragalactic and a galactic component of the diffuse radiation can be identified. The former component, which is essentially isotropic, gives information about processes and developments at large distances from our galaxy, ranging partly back to the early universe. Details about our own galaxy like the interstellar matter, radiation and magnetic fields as well as about the origin and the propagation of galactic cosmic rays can be deduced from investigations of the galactic diffuse emission.

Direct measurements of the diffuse emission in the 30 MeV to 50 GeV energy range are provided by the EGRET experiment [1,2]. At high galactic latitudes an extragalactic component has been observed, a significant fraction of which is attributed to the direct emission from AGNs [3]. The main part of the diffuse emission is concentrated at the galactic disc and the inner galaxy, which therefore points to a galactic origin. The EGRET data below 1 GeV can be well explained by interactions of cosmic-ray electrons and protons with the interstellar radiation field and with the interstellar matter [4]. The dominant interaction processes are π^0 production by nucleon–nucleon interactions, inverse Compton (IC) scattering

with low-energy photons and high-energy electron bremsstrahlung. Above 1 GeV the observed photon flux exceeds the model predictions [1]. A possible explanation for this discrepancy is that the average interstellar proton spectrum is harder than the spectrum observed in the local neighbourhood, leading to a harder π^0 and thus also to a harder diffuse gamma-ray spectrum [5–8]. The discrepancy may also be due to an underestimation of the IC contribution, which starts to become relevant above 1 GeV [9–15]. The favoured hypothesis for an enhanced IC contribution is an average electron spectrum in the galaxy which is substantially harder than that measured locally [10,14,15]. An alternative or additional contribution could be gamma radiation from supernova remnants and pulsars [16].

It is interesting to note that in models with increased IC contribution [13,14] not only the excess of photons above 1 GeV can be explained but also the longitude and latitude profiles up to the galactic poles can be reproduced. This could be relevant for the experimental determinations of the isotropic extragalactic emission.

In these models the IC contribution to the diffuse photon background dominates above 1 GeV. Depending on the cutoff energy for the electron injection spectrum a maximum of the differential photon flux (multiplied by E^3) is predicted between 30 and 200 TeV [11]. For the inner galaxy the flux at the maximum corresponds to a fraction of

$\sim 5 \times 10^{-4}$ of the cosmic ray flux (see Fig. 11). The IC contribution is rather broad in galactic latitude and extends up to the galactic poles, and even there it is comparable to or greater than the expected isotropic extragalactic contribution [13,14].

The broad distribution in galactic latitude is due to the broad distribution of the interstellar radiation field, which is the target field for the IC process. In contrast, a model with enhanced π^0 production would predict a gamma radiation which is more confined to the galactic disc, because of the narrow distribution of the interstellar matter, the target for the π^0 production process. This difference may allow one to distinguish between the two hypotheses.

Contributions to the extragalactic diffuse emission below 100 TeV are expected from the cascading of ultra-high-energy photons and electrons on the cosmic microwave background (CMB), creating eventually a pile-up of gamma rays in the 10–100 TeV region [17,18]. The ultra-high-energy photons and electrons may be decay products of supermassive particles [19], themselves radiated during collapse or annihilation of topological defects [20]. Alternatively they may result from the interaction of ultra-high-energy hadronic cosmic rays with the CMB [21]. The expected level of gamma flux contributed by the cascading process is estimated to be 10^{-5} of the cosmic ray flux [21–23].

In the 1 TeV to 1 PeV energy range there are two experiments which claim the observation of a diffuse photon signal: Refs. [24,25]. The result reported by Ref. [24] is only a 2.8 sigma effect and may therefore well be considered as an upper limit. Moreover, there may be an additional uncertainty of the result due to uncertainties on the muon content of photon showers [26]. The gamma-ray excess reported by Ref. [25] is a 3.8 sigma effect, which may be correlated with the Loop 1 region. In a later publication by the same collaboration [27] only an upper limit of the diffuse gamma-ray flux is given. All other experiments in the 1 TeV to 1 PeV energy region give upper limits on the diffuse photon flux (see Tables 2 and 3 and Figs. 11 and 12).

In the present analysis [28] an independent new determination of an upper limit on the diffuse

photon background is performed in the 20–100 TeV region, where only two other experiments have reported results [29,30], in addition to previous measurements with the HEGRA array [31,32].

The energy region below and around 100 TeV is of particular interest because on the one hand the extragalactic component of the diffuse photon background is expected to contribute predominantly in this energy region. On the other hand, according to some models [11], the ratio $I_\gamma / I_{\mathrm{CR}}$ of the differential diffuse photon flux I_γ of galactic origin to the cosmic ray flux I_{CR} has a maximum in the 100 TeV region (see Figs. 11 and 12).

The paper is structured as follows: Section 2 describes the experimental details, Section 3 the Monte Carlo (MC) simulation. In Section 4 the definition of the data sample to be used in the analysis is given. The measurement of the upper limit on the diffuse photon flux is presented in Section 5 and the results are discussed in Section 6.

2. Experimental details

2.1. The detector

The data were taken with the HEGRA air shower array located at 2200 m a.s.l. on the Canary island La Palma. Since April 1998 the array consisted of 97 wide-angle Cherenkov detectors (AIROBICC) and of 182 scintillation detectors. A fire in October 1997 had destroyed 39 AIROBICC detectors, all of which were rebuilt, and 65 scintillation detectors, of which only four were rebuilt. The two types of detectors measure the Cherenkov radiation and the secondary particles (mainly photons, converted in a 5 mm thick lead plate above the 4 cm thick plastic scintillator sheet, and electrons) respectively, which are produced in air showers induced by primary cosmic rays (including gammas) in the atmosphere. The AIROBICC detectors were distributed over an area of $200 \times 200 \text{ m}^2$. This area contained completely the $150 \times 200 \text{ m}^2$ area covered by the scintillator array. The detectors are described in detail in Refs. [33,34].

The experimental trigger required a time coincidence within 150 ns of $\geqslant 6$ Cherenkov detectors (AIROBICC trigger) or of $\geqslant 14$ scintillation

detectors (scintillator trigger). The trigger rate was 28 Hz on the average.

The data used in this analysis were taken in the period from April 1998 to March 2000. Only data with an AIROBICC trigger have been considered. The total effective observation time amounts to ~1464 h.

2.2. Detector calibration and shower reconstruction

The detectors register the arrival time (*time* data) and the light flux (*amplitude* data) hitting the photocathode of the photomultipliers. For each detector the amplitude is given in terms of the number of ADC channels. In the case of the scintillator array the relative calibration of amplitudes between the individual detectors is done on the basis of the so-called '1-MIP peak'. The 1-MIP peak is the position of the maximum in the ADC spectrum corresponding to the detector response for one minimum ionizing particle [35]. For the Cherenkov array a relative calibration between the individual detectors is achieved by normalizing the high-amplitude tails of the individual ADC spectra to each other [35]. The absolute calibrations of the amplitudes are described in Section 3.2.

By the absolute calibrations the amplitudes are transformed into a density of Cherenkov photons impinging on the surface of the Cherenkov detectors or a density of secondary electrons and photons impinging on the surface of the scintillation detectors respectively.

For each shower the shower direction, the position of the shower core and the Cherenkov light density $\rho(r)$ as a function of the distance r from the shower core were reconstructed by a simultaneous fit (*global AIROBICC fit*) to the time and amplitude data from the Cherenkov detectors. From $\rho(r)$ the Cherenkov light density L_{90} at $r = 90$ m and the light radius $R_{\mathrm{L}} = -1/(\mathrm{d}\ln\rho(r)/\mathrm{d}r)$ in the region 50 m $< r <$ 120 m were derived. The total number N_{s} of photons and electrons at the detector level was determined by a maximum likelihood fit to the particle densities from the scintillation detectors.

L_{90} is known to be a good measure of the shower energy. In the following L_{90} and R_{L} are assumed to

be given in units of (no. of photons/m^2) and (m) respectively.

The quality of the various fits to the time and amplitude data, expressed in terms of χ^2-probabilities and in terms of errors of fitted parameters, is used below in the definition of the selection criteria for the showers.

3. Monte Carlo simulation and data-Monte Carlo comparison

3.1. Monte Carlo simulation

An essential part of the present analysis is the MC simulation of the experiment. The simulation comprises:

- The simulation of the physical processes in the shower development, including the production of Cherenkov photons. The CORSIKA program, version 4.068, was used for this step [37].
- The simulation of the detector. A comprehensive discription is given in Ref. [38].
- The simulation of the chemical composition and of the energy spectrum of the charged cosmic rays. The simulation was based on the compilation [39] (see Table 1).

MC data were generated for primary photons, protons, He–, O– and Fe nuclei, for the zenith angles $\Theta = 10°$, $20°$ and $30°$ and for the energy region 5 TeV $< E <$ 1000 TeV. For each particle type and each zenith angle approximately the same number of showers was generated, giving a total of 133,000 showers. By assigning to each of these showers 20 different core positions, chosen randomly in a 300×300 m^2 area centered at the actual detector array, the statistics of quasi-independent showers was increased by a factor of 20.

The generated showers were given appropriate weights to simulate the expected distributions in E, Θ and the cosmic ray species. For the comparisons with the experimental data an admixture of photons with $\phi_0 = 0.0002582$ (m^2 s sr TeV)$^{-1}$ has been assumed in the MC sample (see Table 1), corresponding to 1/1000 of the hadronic cosmic ray flux at 1 TeV.

Table 1
Absolute differential fluxes $\phi = \phi_0 (E/\text{TeV})^{-\gamma}$ used for the definition of MC samples

Generated particle	$\phi_0 \left(\dfrac{\text{no. of particles}}{\text{m}^2\,\text{s}\,\text{sr}\,\text{TeV}} \right)$	Spectral index (γ)	Sample is representative for	Z
H	0.1091	2.75	H	1
He	0.06808	2.62	He–Li	2–3
O	0.05182	2.65	Be–Si	4–14
Fe	0.02919	2.60	P–Ni	15–28
H–Fe	0.2582	–	Hadrons	1–28
γ	0.0002582	2.75	Photons, e$^+$, e$^-$	–

In the following 'MC events' always means 'weighted MC events'.

3.2. Absolute calibration of N_s and L_{90}

The absolute calibration of N_s and L_{90} is done separately for each subrun (corresponding to 30 min of observation time). The calibration factor for N_s is determined such that $\langle \log_{10}(N_s) \rangle$ in the experimental data agrees with $\langle \log_{10}(N_s) \rangle$ in the MC data. This is done using samples defined by the standard selection criteria (see Section 4).

The absolute N_s calibration defines—through the MC simulation—the absolute energy scale in the experimental data. By comparing with other methods of calibrating N_s, for example using the 1-MIP peak not only for the relative but also for the absolute calibration of N_s [35], the error in the absolute energy scale is estimated to be in the order 20%.

After calibration, the $\log_{10}(N_s)$ distributions of the experimental data and of the MC data agree fairly well (see Fig. 1). There is also reasonable agreement in the total number of showers: for a small subset of runs the total number of showers in the experimental data was compared with the corresponding MC number expected on the basis of the measured on-time and the all-particle cosmic ray flux from Ref. [39]. There is agreement within 7%. This can be regarded as a good consistency between experimental data and MC data, given the fact that already a miscalibration of N_s by 10% would yield a discrepancy in the number of reconstructed showers of $(1.10^{1.7} - 1.0) = 17.6\%$.

The absolute calibration of L_{90} is done using the calibrated N_s values, namely by determining a calibration factor for L_{90} such that $\langle \log_{10}(N_s/L_{90}) \rangle$
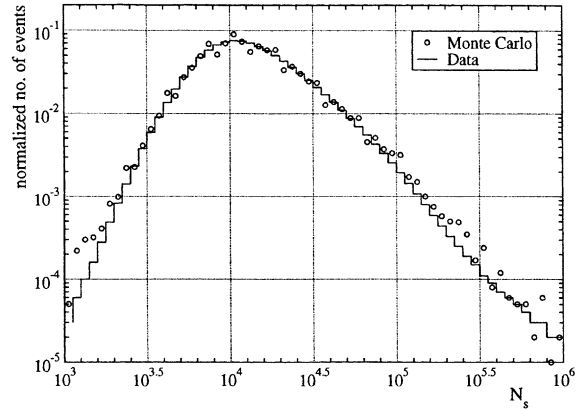

Fig. 1. Distribution of $\log_{10}(N_s)$ for the experimental data (histogram) and for the MC data (open circles).

in the experimental data coincides with $\langle \log_{10}(N_s/L_{90}) \rangle$ in the MC data. The calibration factor is determined separately for each of five bins in the variable $(1/R_L)$.

3.3. Adjustment of errors in the Monte Carlo simulation

A comparison of the fluctuations of arrival times and amplitudes between experimental data and MC data gave good agreement for the data from the scintillation detectors. For the Cherenkov detectors the fluctuations were found to be significantly lower in the MC data than in the experimental data. The difference is explained on the one hand by an underestimation of the average light of the night sky background in the MC simulation. On the other hand, the difference may be due to subtle effects in the conversion chain

from the photons to the final electronic signal, such as variations in the Winston cone reflectivity, non-uniformity in the quantum efficiency and the photoelectron collection efficiency of the photomultipliers, etc. Instead of repeating the MC simulation with a more realistic night sky background and with a refined simulation of the detector non-uniformities, the fluctuations of arrival times and amplitudes from the Cherenkov detectors were randomly increased in the MC-generated data to agree with those in the experimental data. On the average the RMS of the Cherenkov photon densities and that of the Cherenkov photon arrival times was increased by a factor of 1.8.

3.4. Data-Monte Carlo comparison

Some comparison of experimental data and MC data are shown in Figs. 1–4. The data samples are defined by the standard selection criteria listed in Section 4. Because these selection criteria are tighter than the trigger condition no simulation of the trigger was necessary. In each of the Figs. 1–3 the two distributions were normalized to the same total number of events. For $\log_{10}(N_s)$, R_L and also for $\log_{10}(N_s/L_{90})$ versus $(-1/R_L)$ the agreement between data and MC is quite good. A large discrepancy is found for $\log_{10}(L_{90})$ at $\log_{10}(L_{90}) < 4.0$. This may be due to the time dependence of the
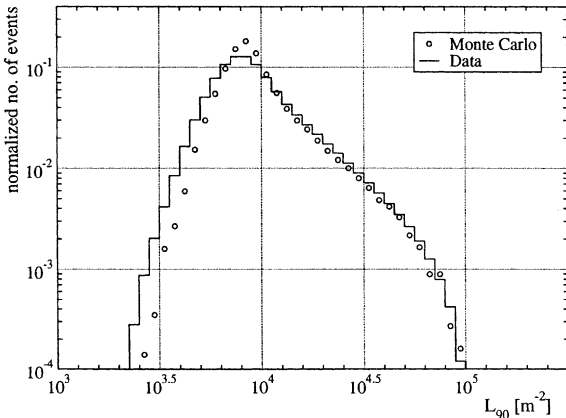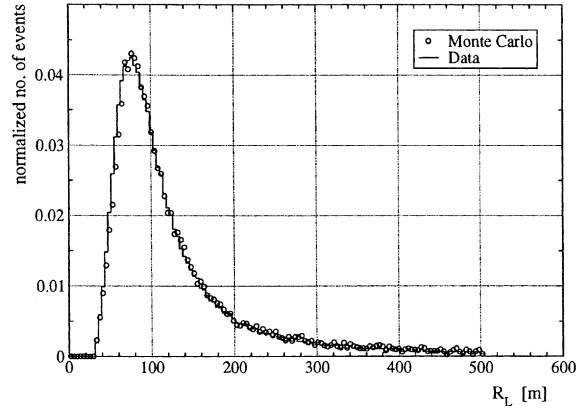

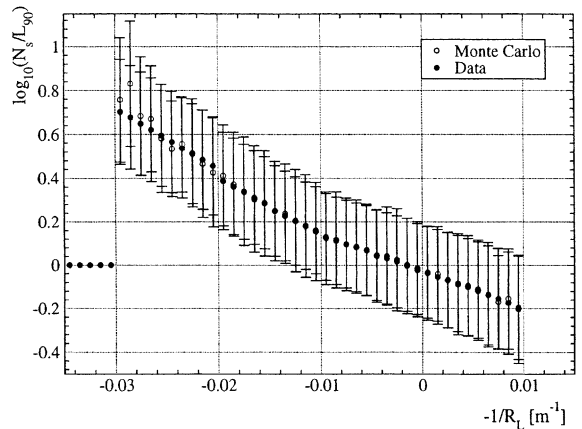Fig. 3. Distribution of R_L for the experimental data (histogram) and for the MC data (open circles).

Fig. 4. Average value of $\log_{10}(N_s/L_{90})$ as a function of $(-1/R_L)$ for the experimental data (full circles) and for the MC data (open circles). The error bars represent the RMS of the $\log_{10}(N_s/L_{90})$ values in each bin of $(-1/R_L)$.

light of the night sky in the experimental data which was not taken into account in the MC simulation.

3.5. Comparison of photon-induced to hadron-induced showers in the Monte Carlo data

An experimental upper limit of the flux of diffuse photons will obviously be the tighter the better photons can be discriminated from hadrons.

Fig. 2. Distribution of $\log_{10}(L_{90})$ for the experimental data (histogram) and for the MC data (open circles).

It is therefore worthwhile searching for measurable quantities which allow a photon–hadron discrimination at least to a certain degree. In the present analysis this is done exclusively with MC data: As no prominent photon signal has been found so far with HEGRA-array data there is no experimental data sample, sufficiently enriched with photons, that could be used for studying the photon–hadron separation.

As shown in Ref. [41] useful variables in this context are $1/R_L$ and the ratio $\log_{10}(N_s/L_{90})$: because hadron-induced showers in general develop more slowly after the shower maximum than photon-induced showers, the ratio $\log_{10}(N_s/L_{90})$ at fixed position of the shower maximum (estimated by $1/R_L$ [40]) is expected to be on the average larger for hadron than for photon showers. This behaviour is illustrated in Fig. 5. The photon–hadron difference is quite independent of $\ln(L_{90})$ and Θ (not shown). In Fig. 4 the experimental data are compared with the MC-(hadron + photon) sample. The agreement for the average $\log_{10}(N_s/L_{90})$ at fixed $(-1/R_L)$ is not surprising because it is the result of the absolute calibrations, described in Section 3.2.

MC studies have shown that the shape parameters of the lateral particle distribution, or alternatively the age parameter in the NKG function,
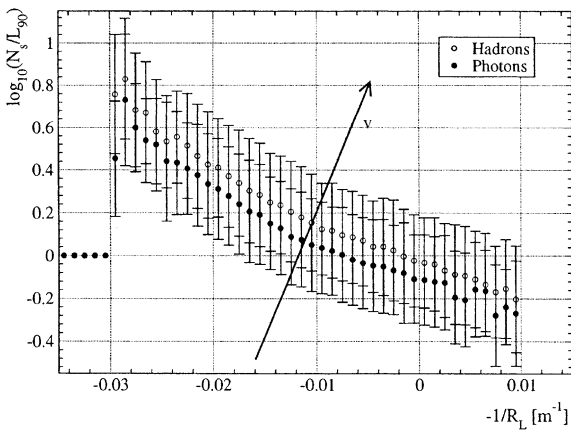

Fig. 5. Average value of $\log_{10}(N_s/L_{90})$ as a function of $(-1/R_L)$ for photon-induced (full circles) and hadron-induced (open circles) showers. The error bars represent the RMS of the $\log_{10}(N_s/L_{90})$ values in each bin of $(-1/R_L)$. The arrow indicates the axis of the variable v defined in the text.

as determined in the fit to the amplitude data from the scintillation detectors, have a potential for discriminating between photons and hadrons which may be superior to that of the variable $1/R_L$. An approach in this direction was followed in Ref. [42]. In the present analysis, however, this potential could not be exploited due to the unsatisfactory results of the comparison between experimental data and MC data: no good agreement was found in the distribution of the age parameter, the distribution being wider and shifted towards lower values in the MC data.

4. Data sample

The aim of the selection criteria is to select well reconstructed showers, to concentrate on energies close to the threshold of the HEGRA array and to retain only data taken under good observation conditions. This is achieved by the set of requirements (called 'standard selections' in the following):

- χ^2-probability of the global AIROBICC fit: $P(\chi^2) > 1\%$,
- zenith angle $\Theta < 35°$,
- -0.03 m^{-1} $< (-1/R_L) < 0.01$ m^{-1},
- fitted errors of the zenith angle Θ and of the azimuthal angle ϕ: $\Delta\Theta < 0.4°$, $\sin\Theta\,\Delta\phi < 0.4°$,
- fitted error on x and y position of the shower core: $\Delta x_{core} < 15$ m, $\Delta y_{core} < 15$ m,
- fitted error on $\ln(L_{90})$: $\Delta\ln(L_{90}) < 0.3$,
- χ^2-probability of the maximum likelihood fit to the lateral particle distribution $(\rho_s(r))$ from the scintillation detectors: $P(\chi^2) > 5\%$,
- fitted error on the total number of particles at the detector level: $\Delta\log_{10}(N_s) < 0.4$,
- rejection of very-high-energy showers:

$$\ln(L_{90}) < 11.0 + 0.45\,\frac{\cos\Theta - \cos(30°)}{\cos(10°) - \cos(30°)}$$

This cut eliminates photon showers above $\sim$320 TeV, proton showers above $\sim$640 TeV and Fe showers above $\sim$1000 TeV. The cut has to be applied in order to ensure consistent conditions for experimental data and MC data, which were generated only up to energies of 1000 TeV.

Out of the 163 million triggered showers 19.3 million pass the standard selections. The number of triggered showers (100%) is reduced to 56%, 36% and 12% by requiring one after another a successful global AIROBICC fit, a successful fit to the lateral particle distribution $\rho_s(r)$ and well reconstructed showers. The strong reduction is explained by the large experimental errors in showers which are close to the energy threshold of the trigger.

The main characteristics of the data sample defined by the standard selections are (see also Figs. 1–4):

- average fitted errors:

$$\langle \Delta x_{\mathrm{core}} \rangle \approx \langle \Delta y_{\mathrm{core}} \rangle = 4.1 \text{ m}$$
$$\langle \Delta \Theta \rangle \approx \langle \sin \Theta \, \Delta \phi \rangle = 0.12°$$
$$\langle \Delta \ln(L_{90}) \rangle = 0.12$$
$$\langle \Delta \log_{10}(N_s) \rangle = 0.12$$
$$\langle \Delta(1/R_L) \rangle = 0.003 \text{ m}^{-1}$$

- average zenith angle $\langle \Theta \rangle = 20°$,
- average $\ln(L_{90}) = 9.16$ (L_{90} in units of no. of photons/m²),
- average $\log_{10}(N_s) = 4.12$.

Applying the standard selections to the MC data one finds:

- the energy region for reconstructed photon showers (10% and 90% quantiles) is 20 TeV $< E_\gamma < 100$ TeV, with an average energy of 53 TeV
- the energy region for reconstructed hadron showers (10% and 90% quantiles) is 40 TeV $< E_h < 210$ TeV, with an average energy of 110 TeV
- the ratio of the number of reconstructed photon showers to the number of reconstructed hadron showers N_γ/N_h is 1/346. Note that the γ/h flux ratio assumed in the MC simulation was 1/1000 at 1 TeV (see Table 1). This apparent suppression (by a factor of $\sim$3) of hadron showers is due to the fact that with respect to L_{90} photon showers of a given energy resemble hadron showers of about twice the energy, where the integrated flux is reduced by a factor of $2^{1.7} \approx 3$.
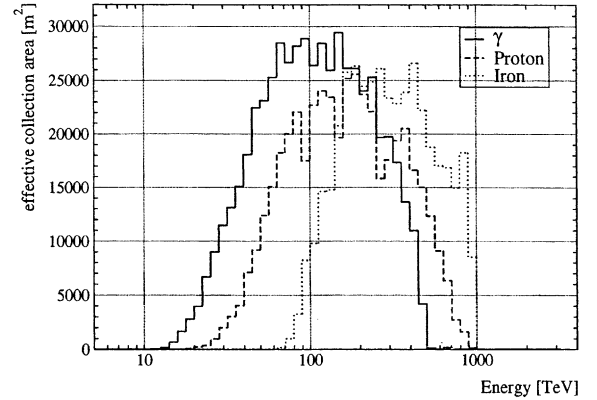

Fig. 6. Effective collection area as a function of the energy for MC showers, after applying the standard selections and averaging over all zenith angles, for photon (solid histogram), proton (dashed histogram) and Fe showers (dotted histogram).

The effective collection area as a function of the energy is shown in Fig. 6 for photon, proton and Fe showers. Defining the threshold energy as the energy where the effective collection area reaches 50% of its maximum value one obtains for photons a threshold energy of 35 TeV, if one averages over all zenith angles, and 22, 28 and 45 TeV for the zenith angles 10°, 20° and 30° respectively.

As can be seen from Figs. 1–4 the average values of the different quantities are similar for experimental data and for MC data. For MC events it has been verified that the average fitted error of Θ is close to the RMS of $(\Theta_{\mathrm{fitted}} - \Theta_{\mathrm{generated}})$. Similar statements hold for other quantities. The value of the average fitted error $\langle \Delta \Theta \rangle \approx 0.12°$ therefore implies that the angular resolution for the data sample defined by the standard selections is around 0.12°, not including possible systematic errors.

In the subsequent analysis the standard selections have always been applied.

5. Determination of upper limits on the flux of diffuse photons

As shown in Section 3.5 some difference between photon and hadron showers is seen in the plot of $\log_{10}(N_s/L_{90})$ versus $(-1/R_L)$ (Fig. 5). Under all projections of the 2-dimensional distribution $\log_{10}(N_s/L_{90})$ versus $(-1/R_L)$ onto some

axis, the one onto the v-axis, indicated by the arrow in Fig. 5, can be expected to yield a relative small overlap between the distributions for photons and hadrons. The distribution in the variable v, defined as

$$v = \log_{10}(N_s/L_{90}(\text{m}^{-2})) + 23.43 \times (0.005 - 1/R_L(\text{m})) \tag{1}$$

will therefore be sensitive to the relative contribution of photons and hadrons.

In the following the distributions of the variable v will be exploited for determining upper limits of the diffuse photon background. Two approaches will be followed

- Determination of a global upper limit by comparing the experimental distribution of v with the MC expectations for primary photons and hadrons (Section 5.1).
- Determination of an upper limit for a specific region in the galaxy by comparing the experimental distributions of v in this region with that of another region in the galaxy (Section 5.2).

5.1. Global upper limit of I_γ/I_{CR}

The distributions in v are denoted as: $q_{\text{data}} = dN_{\text{data}}/dv$ for reconstructed showers of the experimental data, $q_\gamma = dN_{\text{MC}}^\gamma/dv$ for reconstructed MC-photon showers, $q_h = dN_{\text{MC}}^h/dv$ for reconstructed MC-hadron showers.

Both q_h and q_γ are normalized such that they correspond to the absolute distributions of reconstructed MC showers for an effective on-time of 1 s, assuming for photons and hadrons the same differential flux at 1 TeV of 0.2582 particles/ $(\text{m}^2 \text{ s sr TeV})$, which is the measured differential flux of hadronic cosmic rays.

With fixed spectral indices of the photon and hadron fluxes (Table 1) the contribution from photons to the cosmic ray flux may be specified by the ratio $r_0 = I_\gamma^0/I_{CR}^0$ of the differential photon flux and the differential hadron flux at some arbitrary energy E_0. E_0 is chosen as 1 TeV.

The ratio r_0 is then determined by fitting q_{data} by a superposition of q_γ and q_h:

$$q_{\text{data}} = T_{\text{on}}(\text{s})a(q_h + r_0 q_\gamma) \tag{2}$$

T_{on} is the total on-time of the experimental data, and a and r_0 are free parameters to be determined in the fit.

Using the spectral indices adopted in the MC simulation (see Table 1) r_0 can be converted into a ratio r_1 at any other energy E_1 (see below). If one wants to determine in the fit r_1 instead of r_0, the term $r_0 q_\gamma$ in Eq. (2) has to be replaced by $r_1 q_{\gamma,1}$ with $q_{\gamma,1} = q_\gamma r_0/r_1$. The term q_h would remain unchanged, because q_h has been normalized to the measured differential flux of hadronic cosmic rays already. The choice of the reference energy E_0 is therefore completely arbitrary.

In case of a perfect MC simulation and an accurate measurement of the on-time T_{on} the normalization factor a should come out to be 1. Leaving it free in the fit makes the result for r_0 independent of small inconsistencies in normalization between experimental data and MC data and compensates for small deficiencies of the MC simulation.

The distributions q_γ, q_h and q_{data} are displayed in Fig. 7. Due to the expected very small contribution from photons q_{data} and q_h are very similar. However, a closer look reveals that the RMS of
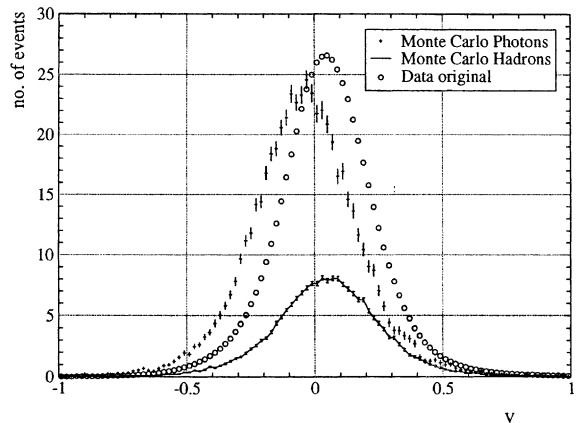

Fig. 7. Distribution of the variable v for MC-photon (crosses) and MC-hadron showers (solid curve). The number on the y-axis is the number of reconstructed showers, after applying the standard cuts, assuming for photons and hadrons the same differential flux at 1 TeV of 0.2582 particles/(m² s sr TeV), the spectral indices listed in Table 1 and an effective on-time of 1 s. The circles represent the v distribution of the experimental data, multiplied by a factor 6×10^{-7}.

q_{data} (0.206) is slightly lower than the RMS of q_{h} (0.224). These larger fluctuations of the MC data could have their origin in the shower simulation or may be due to a slight overestimation of the measurement errors in the MC data (cf. Section 3.3). To correct for this discrepancy the experimental distribution will be smeared by distributing the content of one bin over the same bin and neighbouring bins according to a Gaussian. The sigma s of the Gaussian is determined as third parameter in the fit.

The experimental distribution q_{data} can be well fitted by a superposition of q_{γ} and q_{h}: the χ^2 is 88 for 85 degrees of freedom (Fit A). In Fig. 8 the experimental distribution (points with error bars) is compared with the fitted sum of the contributions from hadrons and photons (dotted curve). The fitted contribution from photons is drawn as solid curve. The distribution of the pulls has an average of 0.21 and an RMS of 0.99. The results for the parameters r_0 and s are

$$r_0 = 0.014 \pm 0.005 \quad s = 0.080 \pm 0.003 \tag{3}$$

The quoted errors correspond to 1.282 sigma, so that $r_0 + \Delta r_0$ is the upper limit of r_0 at the 90% confidence level, taking only the statistical errors into account.

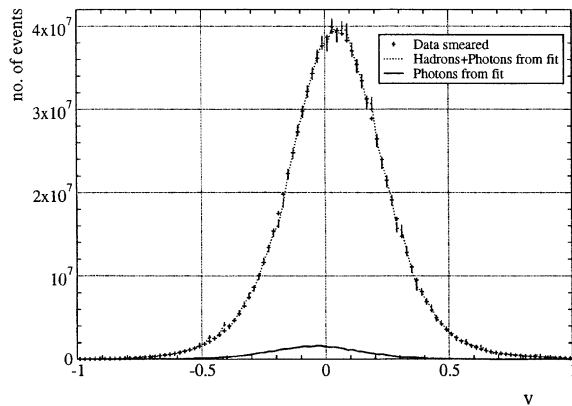To check the stability of the results and to assess the systematics, a and r_0 were also determined

Fig. 8. Distribution of the variable v for the smeared experimental data (points with error bars). The dotted curve represents the fitted sum of the contributions from photons and hadrons, the solid curve the fitted contribution from photons only.

as a function of v_0, where v_0 is the border line between two intervals of v: $v < v_0$ and $v > v_0$. The integrated distribution of q_{data}, q_h and q_γ in the two intervals were used to calculate a and r_0 (solving two equations with two unknowns), keeping s fixed at 0.080. Both a and r_0 are found to be stable (and consistent with the results from Fit A) in the region $-0.18 < v_0 < 0.30$. This is the region which contains the bulk of the showers: 74% of q_{data}, 76% of q_h and 68% of q_γ. For v_0 outside of the above interval a and r_0 are not stable indicating that the tails of the q_{data} distribution are not well represented by the MC simulations.

Changing v_0 from -0.18 to -0.5 results in a change of r_0 from 1.4% to -1.5%. Setting the parameter s to zero in Fit A yields $r_0 = -3.1$% with an unacceptable χ^2 of 465 (for 86 degrees of freedom). Using different variables $((-1/R_{\text{L}})$, $\log_{10}(N_{\text{s}}/L_{90}))$ instead of v gives either unacceptable fits $(\chi^2/(\text{no. of degrees of freedom}) > 2)$ or r_0 values between -3% and 0%. These results suggest that the r_0 from Fit A can be regarded as an upper limit with respect to systematic errors. They also imply that r_0 from Fit A should not be interpreted as a positive photon signal, although r_0 differs from zero by 3.6 standard deviations. If r_0 is fixed at zero in Fit A the χ^2 value increases from 88 to 101, corresponding to a change of the χ^2 probability from 38% to 11%, which is still acceptable. The 90% confidence upper limit of r_0 from Fit A is thus $r_{0,\text{upl}} = r_0 + \Delta r_0 = 1.9 \times 10^{-2}$.

The ratio $r_{0,\text{upl}}$ at 1 TeV is transformed to the average photon energy of the selected data sample of 53 TeV, using the spectral indices of the photon and hadron fluxes adopted in the MC simulation (see Table 1). One obtains

$$\frac{I_\gamma}{I_{\text{CR}}}(\langle E \rangle = 53 \text{ TeV}) < 1.4 \times 10^{-2} \quad \text{at 90 c.l.} \tag{4}$$

The results presented so far were obtained with event samples defined by the standard selections. Another fit was performed using tighter cuts in Θ and $(-1/R_{\text{L}})$: $\Theta < 15°$ and $-0.01 \text{ m}^{-1} < (-1/R_{\text{L}}) < 0.01 \text{ m}^{-1}$.

The motivation for these selections is a stronger suppression of very-high-energy showers (Θ cut) and a rejection of showers with large penetration depths ($(-1/R_{\text{L}})$ cut). The latter cut preferentially

rejects hadron showers because they exhibit larger fluctuations in the shower development. An excellent fit is obtained with $\chi^2 = 46.8$ for 56 degrees of freedom. r_0 and $r_{0,\text{upl}}$ are determined as 0.012 and 0.016 respectively, yielding

$$\frac{I_\gamma}{I_{\text{CR}}}(\langle E \rangle = 31 \text{ TeV}) < 1.2 \times 10^{-2} \quad \text{at 90\% c.l.}$$

(5)

5.2. Upper limit of I_γ/I_{CR} for the inner galaxy

The approach described in the previous section is subject to non-negligible systematic effects due to inconsistencies between the MC simulations and the experimental data. One may bypass these problems by looking for a photon signal using experimental data only. The MC simulation is then only needed to parametrize position and shape of the expected photon contribution and to convert the photon signal (given in terms of numbers of events) into a photon flux.

Since the diffuse gamma radiation of galactic origin is expected to be concentrated at the galactic disc, with a width in the galactic latitude b of a few degrees, it is reasonable to compare the v distribution at low $|b|$ (signal region) with that at higher $|b|$ (background region). A larger contribution of photons in the signal region should then show up as an enhancement in the distribution for the signal region relative to the distribution for the background region.

The acceptance of the HEGRA array depends strongly on the zenith angle Θ (due to the construction of the detectors and due to the varying overburden in the atmosphere) and also on the azimuthal angle ϕ (because the detector plane is not horizontal). In addition, because of the varying atmospheric conditions and because of hardware changes of the detector, the acceptance is a function of the time t.

These are the reasons why a photon signal is not searched by comparing the v distributions in absolute scale but rather by comparing their shapes. It was found, however, that the shapes of the experimental v distributions depend on Θ and ϕ too. In principle this could be due to a non-isotropic photon radiation. However, the variations are very likely to a large extent caused by the same reasons which are also responsible for the systematic variations of the acceptance with Θ, ϕ and t. Therefore, before comparing v distributions from different sky regions, which obviously are taken in different regions of the (Θ, ϕ, t) space, one has to define the two v distributions such that they contain the same systematic effects. This is done in the following way:

The experimental data are divided into 12 bins in $\cos\Theta$, 18 bins in ϕ, 352 bins in t and 22 bins in v. One time bin was defined as the minimum number of full nights, with a total observation time of at least 5 h, corresponding to a right ascension scan of $\geqslant 75°$. Within each bin of $(\cos\Theta, \phi, t)$ the v distributions of photons and hadrons are assumed to be independent of $\cos\Theta$, ϕ and t.

With i denoting the ith bin in the $(\cos\Theta, \phi, t)$ space and j the jth bin of v the following quantities are defined:

n_{ij} no. of events from the signal region falling into the ith bin of $(\cos\Theta, \phi, t)$ and into the jth bin of v

$N_i = \sum_j n_{ij}$
     total no. of signal events in the ith bin of $(\cos\Theta, \phi, t)$

$v_{ij} = n_{ij}/N_i$
     normalized v distribution of events from the signal region in the ith bin of $(\cos\Theta, \phi, t)$

m_{ij} as n_{ij} but for events from the background region

$M_i = \sum_j m_{ij}$
     total no. of background events in the ith bin of $(\cos\Theta, \phi, t)$

$w_{ij} = m_{ij}/M_i$
     normalized v distribution of events from the background region in the ith bin of $(\cos\Theta, \phi, t)$

Because the v distribution in general depends on i, but not on $\cos\Theta$, ϕ and t within each bin of $(\cos\Theta, \phi, t)$, information about different photon contributions in the signal and the background region could be obtained by comparing the v distributions at fixed i. One may also compare v distributions summed over all i, provided the

statistical weights of the v distributions in each bin i are chosen to be the same for the signal and the background region:

The v distribution S_j and its error ΔS_j for the signal region are defined as

$$S_j = \sum_i N_i v_{ij} = \sum_i n_{ij} \qquad (\Delta S_j)^2 = \sum_i n_{ij} \qquad (6)$$

The v distribution B_j and its error ΔB_j for the background region are now constructed as

$$B_j = \sum_i N_i w_{ij} \quad (\Delta B_j)^2 = \sum_i N_i^2 (\Delta w_{ij})^2$$
$$\text{with } (\Delta w_{ij})^2 = m_{ij}(M_i - m_{ij})/M_i^3 \qquad (7)$$

By weighting the v distribution w_{ij} with N_i the systematic effects which are present in S_j are simulated in B_j. Differences between the shapes of the S_j and B_j distributions are now interpreted as being due to different contributions of photons.

This approach is similar to the standard approach proposed by Ref. [43]. However, in contrast to Ref. [43], in the present analysis

(a) the background distribution w_{ij} is not determined from all events but only from those in a well defined sky region, which is different from and has no overlap with the signal region. Therefore signal and background distributions (S_j and B_j respectively) are statistically independent. In addition, the resulting upper limit on the photon contribution is more realistic (in general higher) as compared to the case where signal and background regions do overlap. In the latter case the photon contribution would be underestimated in general.

(b) the background distribution B_j is not constructed by randomly generating a v value from the w_{ij} distribution but rather by using for each observed event the full w_{ij} distribution. In this way full use is made of the measured w_{ij} distribution. Both (a) and (b) make the error calculation simple and transparent.

(c) the sums $\sum_i$ in the calculation of S_j, B_j and their errors extend only over those i for which M_i is greater than N_i. This means that in S_j and B_j only those $(\cos \Theta, \phi, t)$ bins are considered for which the background distribution w_{ij} is at least as well measured as the signal distribution v_{ij}. In partic-

ular, if there are no background events in a certain $(\cos \Theta, \phi, t)$ bin (i.e. $M_i = 0$) then the corresponding events in the signal region (N_i) are not included in the calculation of S_j. The requirement $M_i > N_i$ thus removes possible biases in the comparison of S_j and B_j. Of course, one could think of less restrictive conditions on the bins to be included in the sums, for example demanding M_i to be greater than some positive value, independent of N_i.

The ratio $r_0 = I_\gamma^0/I_{\mathrm{CR}}^0$ at 1 TeV is determined by fitting the signal distribution S_j by a superposition of the background distribution B_j and a term G_j, representing a possible contribution from photons:

$$S_j = a\left(B_j + r_0 \frac{G_j}{\epsilon}\right) \quad (j = 1, \dots, 22) \qquad (8)$$

For G_j the MC expectation q_γ (see above) for reconstructed photon showers, rebinned and normalized to $\sum_i N_i$ reconstructed events, is taken. ϵ is an average ratio of the number of reconstructed hadron to the number of reconstructed photon showers, assuming the same differential flux of photons and hadrons at 1 TeV. The parameters a and r_0 are adjusted in the fit.

The signal and background regions are defined as:

signal region :
$$20° < l < 60° \quad \text{and} \quad |b| < 5°$$
background region :
$$20° < l < 60° \quad \text{and} \quad 10° < |b| < 30°$$

With this definition the average l of the events in the signal region is 48.6° and ϵ is calculated as 0.348. The average l and $|b|$ of the events in the background region is 45.7° and 20° respectively. The results of the fit are:

$$a = 1.0007 \pm 0.0094 \quad r_0 = -(0.0003 \pm 0.0030) \qquad (9)$$

with a χ^2 of 26.6 for 20 degrees of freedom. The signal distribution S_j is compared with the fitted sum of the background distribution (aB_j) and the contribution from photons ($a r_0 G_j/\epsilon$) in Fig. 9.
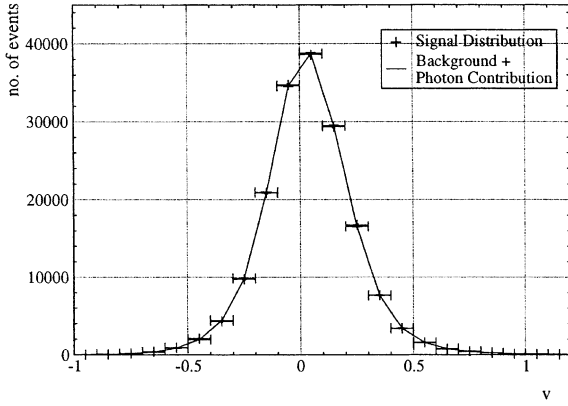
Fig. 9. Distribution S_j of the variable v for the signal region (data points with horizontal bars). The polygon represents the fitted sum of the contributions from the background region (aB_j) and from photons ($ar_0 G_j/\epsilon$).

Transforming r_0 to the average energy of reconstructed photon showers from the signal region of 54 TeV gives the upper limit

$$\frac{I_\gamma}{I_{CR}}(\langle E \rangle = 54 \text{ TeV}) < 2.0 \times 10^{-3} \quad \text{at } 90\% \text{ c.l.}$$

(10)

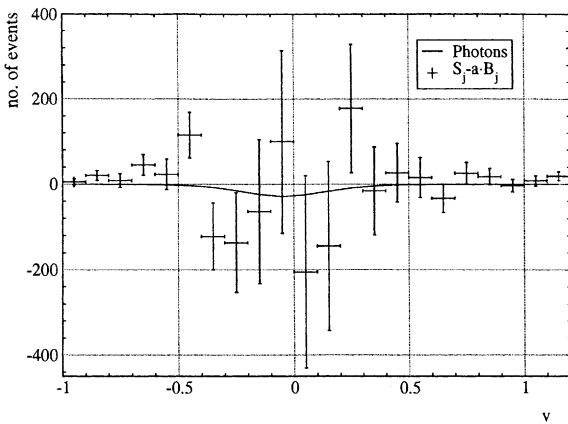The difference ($S_j - aB_j$) is shown in Fig. 10, together with the fitted contribution from photons

Fig. 10. Difference ($S_j - aB_j$) between the v distributions of the signal and the background region (points with error bars). The solid curve represents the fitted contribution from photons ($ar_0 G_j/\epsilon$).

($ar_0 G_j/\epsilon$). The distribution of the pull values has a mean of -0.43 and an RMS of 0.99.

6. Discussion of the results

It should be noted that in the present analysis there is no way of discriminating photon-induced showers from showers induced by electrons or positrons. Therefore the quoted upper limits are limits for the sum of the contributions from photons, electrons and positrons. Extrapolating the differential electron flux (using a spectral index of 3.3), as measured by Ref. [44] between 30 GeV and 1 TeV, and comparing with the predicted flux of diffuse photons at 50 TeV [11] yields an e^-/γ ratio in the order of 10%, at 50 TeV for the inner galaxy. The contribution from positrons is probably an order of magnitude lower than that from electrons [45]. The measured upper limits are therefore in good approximation upper limits of the diffuse photon flux.

The existing measurements of I_γ/I_{CR} in the energy region from 10 GeV to 1 PeV are displayed in Figs. 11 and 12 and compiled in Tables 2 and 3. Fig. 11 displays the measurements which are sensitive to both the isotropic and the non-isotropic component of the diffuse photon flux. The measurements which are sensitive only to the non-isotropic component are plotted in Fig. 12.

With one exception [29], at fixed energy all upper limits in Fig. 11 (Table 2) are bigger than those in Fig. 12 (Table 3). This reflects the larger systematic errors in measurements which are based on absolute comparisons of experimental data with MC predictions. In the experiment [29] the flux and the energy distribution of secondary photons and hadrons is measured at various depths in the atmosphere. It uses the different attenuation lengths for photon-induced showers and for the electromagnetic component of hadron-induced showers to determine an upper limit of I_γ/I_{CR} in the energy region 5 TeV to 1 PeV. In Ref. [31] the experiment is criticized by claiming that the theoretical errors due to uncertainties in the hadronic interaction model and in the chemical composition may be underestimated.
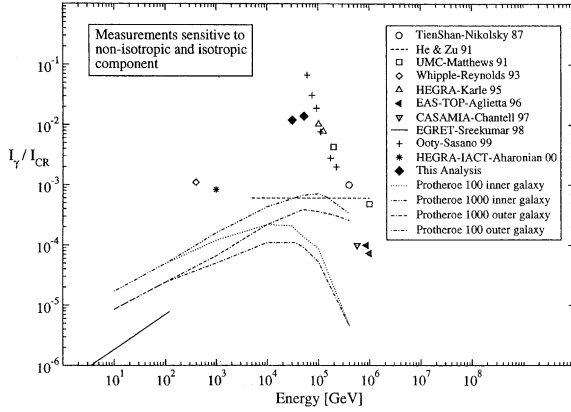
Fig. 11. Comparison of measurements of the ratio I_γ/I_{CR} as a function of the energy in the 10 GeV to 1 PeV range. All data points are upper limits except those from Tien-Shan [24] and from EGRET [2]. The solid line is the EGRET measurement of the isotropic component only. Upper limits are plotted only from those measurements which are sensitive to both the non-isotropic and the isotropic component of the diffuse photon background. The curves represent theoretical predictions by Ref. [11] with the following specifications: cutoff energy of the electron injection spectrum 100 or 1000 TeV respectively, inner galaxy ($-60° < l < 60°, |b| < 10°$) and outer galaxy ($50° < l < 220°, |b| < 10°$) respectively. For all predictions the spectral index of the electron injection spectrum was assumed to be equal to 2.0.
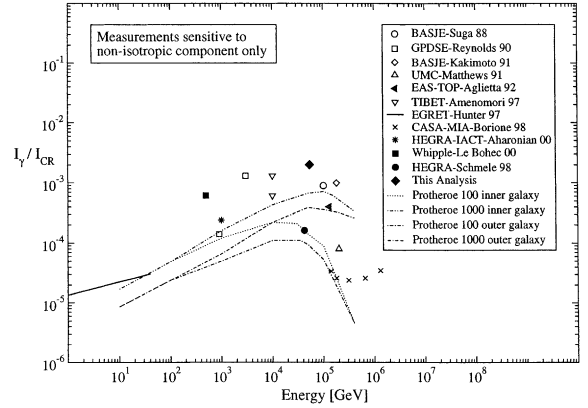
Fig. 12. Comparison of measurements of the ratio I_γ/I_{CR} as a function of the energy in the 10 GeV to 1 PeV range. All data points are upper limits except those from BASJE [25] and from EGRET [1]. The solid line is the EGRET measurement of the non-isotropic component only. Upper limits are plotted only from those measurements which are sensitive to the non-isotropic component of the diffuse photon background only. The curves represent theoretical predictions by Ref. [11] with the following specifications: cutoff energy of the electron injection spectrum 100 or 1000 TeV respectively, inner galaxy ($-60° < l < 60°, |b| < 10°$) and outer galaxy ($50° < l < 220°, |b| < 10°$) respectively. For all predictions the spectral index of the electron injection spectrum was assumed to be equal to 2.0.

Compared to the present analysis the first measurement of a diffuse photon flux obtained from HEGRA-array data [31] was based on a much smaller statistics of experimental data (by a factor of 250) and of MC data (by a factor of 55). In addition the detector consisted of 169 scintillation detectors (now 182) and 49 Cherenkov detectors (now 97). Nevertheless the old result for r is comparable to the new result, which refers to slightly lower energies. In the present analysis more emphasis is put on a good MC tuning. Unfortunately it turns out that because of the increased fluctuations in the MC data (see Section. 3.3) and because of the lower energies, which imply larger errors in the measurements, the potential for a photon–hadron discrimination is clearly reduced.

The upper limits in Fig. 11 (Table 2), including the result of the present analysis, are in general

larger than the theoretical expectations by 1 to 2 orders of magnitude.

The measurements compiled in Fig. 12 (Table 3) are insensitive to the isotropic component of the diffuse photon flux because they are obtained by comparing experimental distributions in a certain sky region (usually low absolute galactic latitudes) with those in a background region (usually larger absolute galactic latitudes).

The measurements provide a good upper limit on the non-isotropic component of the diffuse photon flux only if this component is negligible in the background region. Otherwise the upper limits will in general be too low. In the present analysis the background region is well separated from the signal region (5° in galactic latitude) in order to fullfill this condition. Note that if the IC process is dominating [9,13,14] a rather broad distribution of the diffuse photon flux in the galactic latitude is expected, in which case a good separation between signal and background region is even more critical.

Table 2
Measurements of I_γ/I_{CR} in the 10 GeV to 1 PeV energy range which are sensitive to both the isotropic and the non-isotropic component of the diffuse photon flux

Experiment	References	E_γ	I_γ/I_{CR}	Special selections
Tien-Shan-ASA	[24]	>400 TeV	$(1.0 \pm 0.3) \times 10^{-3}$	$b > 50°$
Emulsion	[29]	5 TeV to 1 PeV	$<6 \times 10^{-4}$	
UMC-ASA	[46]	>200 TeV	$<4.3 \times 10^{-3}$	
		>1000 TeV	$<4.8 \times 10^{-4}$	
Whipple-IACT	[47]	>400 GeV	$<1.1 \times 10^{-3}$	
HEGRA-ASA	[31]	65–160 TeV	$<1.0 \times 10^{-2}$	
		80–200 TeV	$<7.8 \times 10^{-3}$	
EAS-TOP-ASA	[48]	>1000 TeV	$<7.3 \times 10^{-5}$	
		>870 TeV	$<1 \times 10^{-4}$	
CASA-MIA	[49]	>575 TeV	$<10^{-4}$	
EGRET	[2]	10 GeV	1.8×10^{-6}	Out of GPl
		100 GeV	7.0×10^{-6}	Out of GPl
Ooty-ASA	[30]	61 TeV	$<6.7 \times 10^{-2}$	
		76 TeV	$<3.1 \times 10^{-2}$	
		93 TeV	$<1.9 \times 10^{-2}$	
		112 TeV	$<7.6 \times 10^{-3}$	
		175 TeV	$<2.8 \times 10^{-3}$	
		227 TeV	$<2.0 \times 10^{-3}$	
HEGRA-IACT	[50]	1 TeV	$<8.3 \times 10^{-4}$	GPl, $37° < l < 43°$, $|b| < 5°$
HEGRA-ASA	This analysis	31 TeV	$<1.2 \times 10^{-2}$	
		53 TeV	$<1.4 \times 10^{-2}$	

For transforming absolute fluxes into relative fluxes a cosmic ray flux of $I_{CR} = 0.2582 \times (E/\text{TeV})^{-2.68}$ $(\text{m}^2\,\text{s}\,\text{sr}\,\text{TeV})^{-1}$ has been assumed. All data points are upper limits except those from Tien-Shan [24] and from EGRET [2]. The EGRET results are those for the isotropic component only. l and b denote the galactic longitude and latitude respectively. Abbreviations—ASA: air-shower array, IACT: imaging air Cherenkov telescope, GPl: galactic plane.

The upper limit from this analysis is still compatible with the theoretical predictions shown in Fig. 12. The measurements from Refs. [32,46,55] on the other hand suggest that in the model by Ref. [11] the cutoff energy of the electron injection spectrum is well below 1000 TeV.

The result from Ref. [32] is another HEGRA measurement in which only data from the scintillation detectors were used. In that analysis the lack of any gamma–hadron discrimination is more than compensated by the very large data sample, collected during $2\frac{2}{3}$ years of data taking (day and night). In contrast to the data from the Cherenkov detectors, the data from the scintillation detectors depend on the atmospheric conditions (pressure and temperature) in a well controllable way and are practically insensitive to other conditions like the humidity of the air and the presence of clouds.

It should be emphasized that the measurements compiled in Table 3 and plotted in Fig. 12 do not refer to the same sky regions and are therefore strictly speaking not directly comparable. This should also be kept in mind when the experimental upper limits are compared with the theoretical predictions, which are for very specific sky regions.

Acknowledgements

Table 3
Measurements of I_γ/I_{CR} in the 10 GeV to 1 PeV energy range which are sensitive to the non-isotropic component of the diffuse photon flux only

Experiment	References	E_γ	I_γ/I_{CR}	Special selections
BASJE-ASA	[25]	>100 TeV	8.9×10^{-4}	$-40° < \delta < 0$, $180° < \alpha < 210°$
GPDSE	[51]	>900 GeV	$<1.4 \times 10^{-4}$	GPl, $|b| < 5°$
		>3 TeV	$<1.3 \times 10^{-3}$	GPl, $|b| < 5°$
BASJE-ASA	[27]	>180 TeV	$<9.9 \times 10^{-4}$	$-40° < \delta < 0$, $180° < \alpha < 210°$
UMC-ASA	[46]	>200 TeV	$<8.0 \times 10^{-5}$	GPl, $30° < l < 220°$, $|b| < 10°$
EAS-TOP-ASA	[52]	>130 TeV	$<4 \times 10^{-4}$	GPl, $|b| < 5°$
TIBET-ASA	[53]	10 TeV	$<6.1 \times 10^{-4}$	GPl, $140° < l < 225°$, $|b| < 5°$
		10 TeV	$<1.3 \times 10^{-3}$	GPl, $20° < l < 55°$, $|b| < 5°$
EGRET	[1]	17 GeV	2.5×10^{-5}	GPl, $300° < l < 60°$, $|b| < 10°$
		39 GeV	3.0×10^{-5}	GPl, $300° < l < 60°$, $|b| < 10°$
HEGRA-ASA	[32,54]	>42 TeV	$<1.6 \times 10^{-4}$	GPl, $0° < l < 255°$, $|b| < 5°$
CASA-MIA	[55]	140 TeV	$<3.4 \times 10^{-5}$	GPl, $50° < l < 200°$, $|b| < 5°$
		180 TeV	$<2.6 \times 10^{-5}$	GPl, $50° < l < 200°$, $|b| < 5°$
		310 TeV	$<2.4 \times 10^{-5}$	GPl, $50° < l < 200°$, $|b| < 5°$
		650 TeV	$<2.6 \times 10^{-5}$	GPl, $50° < l < 200°$, $|b| < 5°$
		1300 TeV	$<3.5 \times 10^{-5}$	GPl, $50° < l < 200°$, $|b| < 5°$
HEGRA-IACT	[50]	1 TeV	$<2.4 \times 10^{-4}$	GPl, $37° < l < 43°$, $|b| < 2°$
Whipple-IACT	[56]	>500 GeV	$<6.1 \times 10^{-4}$	GPl, $38.5° < l < 41.5°$, $|b| < 2°$
HEGRA-ASA	This analysis	54 TeV	$<2.0 \times 10^{-3}$	GPl, $20° < l < 60°$, $|b| < 5°$

For transforming absolute fluxes into relative fluxes a cosmic ray flux of $I_{CR} = 0.2582 \times (E/\mathrm{TeV})^{-2.68} (\mathrm{m^2\,s\,sr\,TeV})^{-1}$ has been assumed. All data points are upper limits except those from BASJE [25] and from EGRET [1]. The EGRET results are those for the non-isotropic component only. l and b denote the galactic longitude and latitude respectively. δ and α are declination and right ascension respectively. Abbreviations—ASA: air-shower array, IACT: imaging air Cherenkov telescope, GPDSE: galactic plane drift scan experiment, GPl: galactic plane.

References

[1] S.D. Hunter et al., Astrophys. J. 481 (1997) 205.
[2] P. Sreekumar et al., Astrophys. J. 494 (1998) 523.
[3] J. Chiang, R. Mukherjee, Astrophys. J. 496 (1998) 752.
[4] D.L. Bertsch et al., Astrophys. J. 416 (1993) 587.
[5] M. Mori, Astrophys. J. 478 (1997) 225.
[6] P. Gralewicz et al., Astronom. Astrophys. 318 (1997) 925.
[7] I.V. Moskalenko et al., Astronom. Astrophys. 338 (1998) L75.
[8] F.A. Aharonian, A.M. Atoyan, Astronom. Astrophys. 362 (2000) 937.
[9] T.A. Porter, R.J. Protheroe, J. Phys. G. 23 (1997) 1765.
[10] M. Pohl, J.A. Esposito, Astrophys. J. 507 (1998) 327.
[11] T.A. Porter, R.J. Protheroe, Proceedings of the 26th ICRC, Salt Lake City, 1999, OG, 3.2.38.
[12] A.W. Strong et al., ApL 38 (1999) 445.
[13] A. Dar, A. De Rujula, 2000, astro-ph/0005080.
[14] A.W. Strong et al., Astrophys. J. 537 (2000) 763.
[15] I.V. Moskalenko, A.W. Strong, Ap&SS 272 (2000) 247.
[16] E.G. Berezhko, H.J. Völk, Astrophys. J. 540 (2000) 923.
[17] C.T. Hill, D.N. Schramm, Phys. Rev. D. 31 (1985) 564.
[18] V.S. Berezinsky, S.T. Grigor'eva, Astron. Astrophys. 199 (1998) 1.
[19] G. Sigl et al., Astropart. Phys. 2 (1994) 401.
[20] F.A. Aharonian et al., Phys. Rev. D. 46 (1992) 4188.
[21] F. Halzen et al., Phys. Rev. D. 41 (1990) 342.
[22] R.J. Protheroe, T. Stanev, Phys. Rev. Lett. 77 (1996) 3708.
[23] G. Sigl et al., 1996, astro-ph/9604093 v2.
[24] S.I. Nikolsky et al., J. Phys. G. 13 (1987) 883.
[25] K. Suga et al., Astrophys. J. 326 (1988) 1036.
[26] M. Drees, F. Halzen, Phys. Rev. Lett. 61 (1988) 275.
[27] F. Kakimoto et al., Proceedings of the 22nd ICRC, Dublin, vol. 1, 1991, p. 412.
[28] S. Denninghoff, Ph.D. Thesis, Technische Universität München, 2001.
[29] Y.D. He, R.Q. Zhu, Phys. Rev. D. 44 (1991) R2635.
[30] M. Sasano et al., Proceedings of 26th ICRC, Salt Lake City, 1999, OG, 2.4.14.
[31] A. Karle et al., Phys. Lett. B 347 (1995) 161.
[32] D. Schmele, Ph.D. Thesis, Universität Hamburg, 1998.
[33] M. Merck, Ph.D. Thesis, Ludwigs-Maximilians-Universität München, 1993.
[34] A. Karle et al., Astropart. Phys. 3 (1995) 321.
[35] A. Moralejo, Ph.D. Thesis, Universidad Complutense de Madrid, 2000.

[37] J.N. Capdevielle et al., KfK Report 4998, Institut für Kernphysik, Karlsruhe, 1992.
[38] S. Martínez et al., Nucl. Instrum. Meth. A 357 (1995) 567.
[39] B. Wiebel-Sooth et al., Astronom. Astrophys. 330 (1998) 389.
[40] J.R. Patterson, A.M. Hillas, J. Phys. G. 9 (1983) 1433.
[41] F. Arqueros et al., Astropart. Phys. 4 (1996) 309.
[42] J. Prahl, Ph.D. Thesis, Universität Hamburg, 1999.
[43] D.E. Alexandreas et al., Nucl. Instrum. Meth. A. 328 (1993) 570.
[44] J. Nishimura et al., Astrophys. J. 238 (1980) 394.
[45] J.A. Musser et al., Proceedings of the 25th ICRC, Durban, vol. 4, 1997, p. 209.
[46] J. Matthews et al., Astrophys. J. 375 (1991) 202.
[47] P.T. Reynolds et al., Astrophys. J. 404 (1993) 206.
[48] M. Aglietta et al., Astropart. Phys. 6 (1996) 71.
[49] M.C. Chantell et al., Phys. Rev. Lett. 79 (1997) 1805.
[50] F.A. Aharonian et al., Astronom. Astrophys. 375 (2001) 1008.
[51] P.T. Reynolds et al., Proceedings of the 21st ICRC, Adelaide, vol. 2, 1990, p. 383.
[52] M. Aglietta et al., Astrophys. J. 397 (1992) 148.
[53] M. Amenomori et al., Proceedings of the 25th ICRC, Durban, vol. 3, 1997, p. 117.
[54] D. Horns, D. Schmele, Proceedings of the 26th ICRC, Salt Lake City, OG, 1999, 3.2.24.
[55] A. Borione et al., Astrophys. J. 493 (1998) 175.
[56] S. LeBohec et al., 2000, astro-ph/0003265.